mathematics

MDPI

Article

Analysis of Heat Transfer for the Copper–Water Nanofluid Flow through a Uniform Porous Medium Generated by a Rotating Rigid Disk

Naif Abdulaziz M. Alkuhayli [1] and Andrew Morozov [2,3,*]

[1] Mathematics Department, College of Science, Jouf University, Sakaka P.O. Box 2014, Saudi Arabia; naalkuhayli@ju.edu.sa
[2] School of Computing and Mathematical Sciences, University of Leicester, Leicester LE1 7RH, UK
[3] Institute of Ecology and Evolution, Russian Academy of Sciences, Leninsky pr. 33, Moscow 117071, Russia
* Correspondence: am379@leicester.ac.uk

Abstract: This study theoretically investigates the temperature and velocity spatial distributions in the flow of a copper–water nanofluid induced by a rotating rigid disk in a porous medium. Unlike previous work on similar systems, we assume that the disk surface is well polished (coated); therefore, there are velocity and temperature slips between the nanofluid and the disk surface. The importance of considering slip conditions in modeling nanofluids comes from practical applications where rotating parts of machines may be coated. Additionally, this study examines the influence of heat generation on the temperature distribution within the flow. By transforming the original Navier–Stokes partial differential equations (PDEs) into a system of ordinary differential equations (ODEs), numerical solutions are obtained. The boundary conditions for velocity and temperature slips are formulated using the effective viscosity and thermal conductivity of the copper–water nanofluid. The dependence of the velocity and temperature fields in the nanofluid flow on key parameters is investigated. The major findings of the study are that the nanoparticle volume fraction significantly impacts the temperature distribution, particularly in the presence of a heat source. Furthermore, polishing the disk surface enhances velocity slips, reducing stresses at the disk surface, while a pronounced velocity slip leads to distinct changes in the radial, azimuthal, and axial velocity components. The study highlights the influence of slip conditions on fluid velocity as compared to previously considered non-slip conditions. This suggests that accounting for slip conditions for coated rotating disks would yield more accurate predictions in assessing heat transfer, which would be potentially important for the practical design of various devices using nanofluids.

Keywords: copper–water nanofluid; polished rotating disk; velocity slip; temperature slip; effective viscosity; heat source

MSC: 35Q30; 55P05; 76M45

Citation: Alkuhayli, N.A.M.; Morozov, A. Analysis of Heat Transfer for the Copper–Water Nanofluid Flow through a Uniform Porous Medium Generated by a Rotating Rigid Disk. *Mathematics* **2024**, *12*, 1555. https://doi.org/10.3390/math12101555

Academic Editor: Xiangmin Jiao

Received: 1 April 2024
Revised: 4 May 2024
Accepted: 10 May 2024
Published: 16 May 2024

1. Introduction

Nanofluids, as a research area, have attracted much attention over the past couple of decades due to their widespread applications. From modern drug delivery systems to advanced domestic and industrial temperature control systems, nanofluids find use in almost all activities of life. In particular, nanofluids are largely applied in microbiology and medicine due to their extraordinary and targeted thermophysical, chemical, and antibacterial properties [1]. Advanced synthesis mechanisms for nanoparticles have enabled us to achieve the precise thermophysical characteristics required for specific processes. Pioneering work by Choi and Eastman [2] on modeling the thermal properties of nanofluids has been largely extended by a number of studies, including those by Buongiorno [3] and Tiwari and Das [4]. Further, Nield and Kuznetsov [5] proposed a revised model for the

thermal instability of nanofluids. Abbasi et al. [6,7] suggested a few promising models for efficient drug delivery systems using a peristaltic flow of nanofluids. Recently, different artificial intelligence (AI) methods have emerged as powerful tools in nanofluid research, offering new avenues for modeling, prediction, and optimization. Recent studies [8,9] have explored the application of AI techniques to various aspects of nanofluid research, strengthening the application of nanofluids in emerging technology. AI algorithms, such as machine learning, deep learning, and neural regression, have been utilized to analyze experimental data, predict nanofluid behavior, and optimize the choice of parameters. By leveraging AI methods, one can overcome traditional limitations in modeling nanofluids, leading to more efficient and reliable nanofluid-based technologies [10–16].

Among other important scenarios, the dynamics of nanofluids in flows generated by the rotation of a circular disk has been intensively studied in the literature. The analysis of flows generated by a rotating disk was initiated by classical work by Von Kármán [17], who used the radial symmetry of a steady flow to propose so-called similarity transformations for the flow velocity. Modifications to Kármán's work were made by Cochran [18]. Stuart [19] studied the flow due to a porous rotating disk. Turkyilmazoglu [20] presented an analysis of the flow of a nanofluid over a rotating disk. Turkyilmazoglu [21] analyzed the flow due to a rotating and vertically moving disk. Mustafa [22] considered the flow due to a rotating disk using "Buongiorno's model" with slip effects, i.e., the scenario with relative movement between the disk and the fluid. The mentioned study assumed a constant magnetic field applied to the nanofluid. Among other conclusions, the authors reported that all the velocity components of the nanofluid should be decreasing functions of the slip parameter.

Despite a general appreciation of the importance of the slip boundary conditions in modeling nanofluids ([23–26]), there is still a major gap in our understanding of the behavior of their velocity and temperature distributions, even for classical scenarios of generating flow, such as in the case of a uniformly rotating disk. The current theoretical study is designed to partly bridge the above-mentioned gap. Namely, we simulate the velocity and temperature fields of a system of copper–water nanofluid in a flow generated by a polished (coated) rotating disk. Copper–water nanofluids have important practical applications, particularly in thermal conductivity [27–30]. The smoothness of the disk results in velocity and thermal slips. The nanofluid is assumed to be flowing through a porous medium possessing uniform porosity, and we also consider the effects of the generation of heat within the flow.

Mathematically, we reduce the original 3D system of Navier–Stokes PDEs to a set of ODEs using the similarity transformations devised by Von Kármán for a steady flow. Then, we apply numerical simulations to solve the obtained boundary value problem for realistic values of parameters corresponding to typical copper–water nanofluids, taken from the literature. We find that the velocity and temperature slip parameters have a considerable impact on the spatial distribution of the temperature and velocity in the porous media. We also obtain that for the slip condition scenario, the fluid velocity demonstrates a distinct dependence on some key model parameters (e.g., the nanoparticle fraction), as compared to the previously considered non-slip condition for the same system of rotating nanofluids. Possible applications of the current investigation might involve the implementation of nanofluids in turbine engineering, rotor–stator systems, rotational air filters, chemical engineering, centrifugal pumps, and aerospace engineering, where the coating of rotating disks occurs.

2. Materials and Methods

2.1. Model Equations

We consider the flow of a nanofluid composed of copper nanoparticles of a spherical shape uniformly distributed in water on the top of a circular disk. The physical model and the boundary conditions are shown in Figure 1. The volume fraction of the nanoparticles is denoted by ϕ. The disk rotates at a uniform circular velocity, ω, in its own plane, and

this causes the fluid to flow. A uniform, porous medium possessing porosity p_1 fills the space above the disk and perturbs the fluid flow. The disk is assumed to be rigid; hence, no flow occurs across its surface. Importantly, the surface of the disk remains at a uniform temperature, T_s, and is polished in a manner so that there exist velocity and temperature slips between the nanofluid and the surface of the disk.

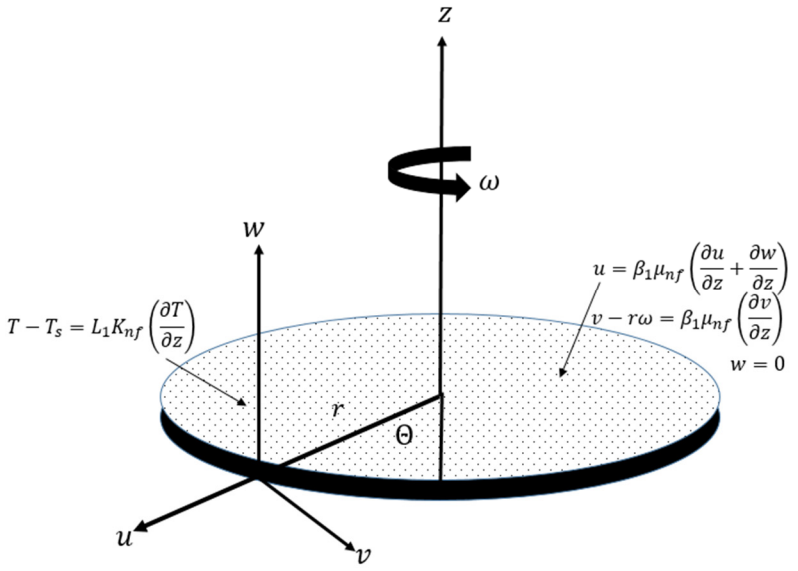

Figure 1. Schematic diagram of the present model along with the boundary conditions.

A cylindrical coordinate system (r, Θ, z) is chosen for modeling the given system, with the disk rotating in the $z = 0$ plane and fluid occupying the space $z \geq 0$. A 3D velocity field of the form $\overline{V} = [u(r, \Theta, z), v(r, \Theta, z), w(r, \Theta, z)]$ is generated due to the rotation of the disk (we assume the flow to be steady). The radial symmetry of the flow is assumed; therefore, all variables become independent of the Θ coordinate. The flow is assumed to be steady. The governing equations for the flow configuration stated above are given as follows [17–22]:

$$\frac{1}{r}\frac{\partial}{\partial r}(ur) + \frac{\partial w}{\partial z} = 0, \tag{1}$$

$$\rho_{nf}\left(u\frac{\partial u}{\partial r} + w\frac{\partial u}{\partial z} - \frac{v^2}{r}\right) = -\frac{\partial p}{\partial r} + \mu_{nf}\left(\frac{\partial^2 u}{\partial r^2} + \frac{1}{r}\frac{\partial u}{\partial r} + \frac{\partial^2 u}{\partial z^2} - \frac{u}{r^2}\right) - \frac{\mu_{nf}}{p_1}u, \tag{2}$$

$$\rho_{nf}\left(u\frac{\partial v}{\partial r} + w\frac{\partial v}{\partial z} + \frac{uv}{r}\right) = \mu_{nf}\left(\frac{\partial^2 v}{\partial r^2} + \frac{1}{r}\frac{\partial v}{\partial r} + \frac{\partial^2 v}{\partial z^2} - \frac{v}{r^2}\right) - \frac{\mu_{nf}}{p_1}v, \tag{3}$$

$$\rho_{nf}\left(u\frac{\partial w}{\partial r} + w\frac{\partial w}{\partial z}\right) = -\frac{\partial p}{\partial z} + \mu_{nf}\left(\frac{\partial^2 w}{\partial r^2} + \frac{1}{r}\frac{\partial w}{\partial r} + \frac{\partial^2 w}{\partial z^2}\right) - \frac{\mu_{nf}}{p_1}w, \tag{4}$$

$$(\rho Cp)_{nf}\left(u\frac{\partial T}{\partial r} + w\frac{\partial T}{\partial z}\right) = K_{nf}\frac{\partial^2 T}{\partial z^2} + \delta. \tag{5}$$

Here, ρ denotes the density, p the pressure, K the thermal conductivity, Cp the specific heat, δ the dimensional heat generation/absorption, and μ the viscosity. The subscript 'nf' stands for the nanofluid. The temperature of the nanofluid, T, is assumed to vary in the axial direction alone since the surface of the disk is maintained at a uniform temperature.

To be able to solve the given fluid dynamics problem, we need empirical relations for the density, viscosity, heat capacity, and thermal conductivity of the copper–water nanofluid, which are taken from previous studies [6,13,14,20].

$$\rho_{nf} = \rho_p\phi - (\phi-1)\rho_f,\ \mu_{nf} = \frac{\mu_f}{(1-\phi)^{2.5}},\ (\rho C)_{nf} = (\rho C)_p\phi - (\phi-1)(\rho C)_f,\ \frac{K_{nf}}{K_f} = \left(\frac{K_p + 2\phi\left(K_p - K_f\right) + 2K_f}{K_p - \phi\left(K_p - K_f\right) + 2K_f}\right). \tag{6}$$

Here, the subscripts 'p' and 'f' denote the nanoparticles and the fluid phase, respectively. We consider spherical-shaped nanoparticles with a size of less than 100 nm. The values of thermophysical quantities of copper and water are given in Table 1.

Table 1. Thermophysical properties of copper and water [24].

	ρ(kg.m^{-3}), Density	K(W.(m.K)$^{-1}$), Thermal Conductivity	Cp(J.(kg.K)$^{-1}$), Specific Heat
Copper	8933	401	385.0
Water	997.1	0.613	4179

The fact that the surface of the disk is rigid facilitates the existence of a slip both in velocity and temperature. Mathematically, this is described by the following boundary conditions. For the radial component of velocity,

$$u = \beta_1\mu_{nf}\left(\frac{\partial u}{\partial z} + \frac{\partial w}{\partial z}\right),\ \ as\ z \to 0, \tag{7}$$

for the azimuthal component of velocity,

$$v - r\omega = \beta_1\mu_{nf}\left(\frac{\partial v}{\partial z}\right),\ as\ z \to 0, \tag{8}$$

for the axial component of velocity,

$$w = 0,\ \ as\ z \to 0, \tag{9}$$

for the temperature,

$$T - T_s = L_1K_{nf}\left(\frac{\partial T}{\partial z}\right),\ as\ z \to 0, \tag{10}$$

and far away from the disk (i.e., as $z \to \infty$), we have

$$u = v = w = 0,\ T = T_\infty. \tag{11}$$

Here, β_1 and L_1 are the dimensional velocity slip and thermal slip parameters, respectively. The velocity slip parameter, β_1, is the relative motion, or slip, between the fluid and the rotating disk surface, which measures how far the fluid's surface velocity and the rotating disk's velocity diverge. The temperature slip parameter describes the variation in temperature between the fluid and the disk surface. In particular, it shows how far the fluid temperature is from the disk surface temperature.

We would like to stress that despite there being few available studies accounting for the slip effects of the flow of nanofluids over a rotating rigid disk (e.g., [26–29]), as mathematically formulated above, the effects of the effective viscosity and thermal conductivity of nanofluids have not been duly investigated. On the other hand, the coating (polishing) of rotating disks occurs in a large number of real-world situations. Thus, the present study is supposed to partly fill the existing void and serve as a reference point for future investigations related to similar flow configurations.

2.2. Similarity Transformations

As per Kármán's deductions, $\frac{u}{r}$, $\frac{v}{r}$, and w become functions of the axial coordinate alone. We apply the following similarity transformations [17–22]:

$$\begin{aligned}(u, v, w) &= \left(r\omega F(\zeta),\ r\omega G(\zeta),\ \left(\omega\nu_f\right)^{\frac{1}{2}} H(\zeta)\right),\\ (p, T) &= \left(p_\infty - \omega\mu_f p(\zeta),\ \ T_\infty + (T_s - T_\infty)\theta(\zeta)\right).\end{aligned} \tag{12}$$

Here, $\zeta\left(= z\left(\frac{\omega}{\nu_f}\right)^{\frac{1}{2}}\right)$ is a new dimensionless variable, and $F(\zeta)$, $G(\zeta)$, and $H(\zeta)$ are dimensionless functions of ζ. By invoking Equation (12), Equations (2)–(5) can be reduced to the following form:

$$A_1F''(\zeta) - A_2\left(F^2(\zeta) + H(\zeta)F'(\zeta) - G^2(\zeta)\right) - \lambda A_1F(\zeta) = 0, \tag{13}$$

$$A_1G''(\zeta) - A_2\left(2F(\zeta)G(\zeta) + H(\zeta)G'(\zeta)\right) - \lambda A_1G(\zeta) = 0, \tag{14}$$

$$A_1H''(\zeta) - P'(\zeta) - A_2H(\zeta)H'(\zeta) - \lambda A_1H(\zeta) = 0, \tag{15}$$

$$A_3\theta''(\zeta) - PrA_4H(\zeta)\theta'(\zeta) + Pr\epsilon = 0, \tag{16}$$

where $\lambda = \left(\frac{\nu_f}{p_1\omega}\right)$ is a dimensionless porosity parameter, $Pr = \left(\frac{\nu_f\left(\rho C_p\right)_f}{K_f}\right)$ is the Prandtl number, and $\epsilon = \left(\frac{\delta}{(T_s - T_\infty)\left(\rho C_p\right)_f\omega}\right)$ is a dimensionless heat generation parameter. Substituting (12) into the continuity equation, Equation (1), suggests that $F(\zeta) = -\frac{H'(\zeta)}{2}$.

The boundary conditions become

$$\begin{aligned}F(\zeta) = \alpha A_1F'(\zeta),\ \ H(\eta) = 0,\ G(\zeta) - 1 = \alpha A_1G'(\zeta),\ \theta(\zeta) - 1 = \beta A_3\theta'(\zeta),\ as\ \eta \to 0,\\ \text{and}\ \ F(\zeta),\ G(\zeta), \theta(\zeta) \to\ 0\ as\ \eta \to \infty.\end{aligned} \tag{17}$$

Here, α and β are the dimensionless velocity slip and temperature slip parameters, respectively. The heat transfer rate and stresses at the surface of the disk are quantities of interest. Therefore, numerical values are presented for such quantities in Tables 2 and 3 for variations in different parameters whose ranges are taken from some related previous studies, such as [22,23,31].

Table 2. Impacts of different parameters on heat transfer rate at the surface of the disk.

α	ϕ	λ	β	$A_3\theta'(0)$
0.00	0.1	1.0	0.05	13.93110
0.05	-	-	-	14.13065
0.10	-	-	-	14.30566
0.05	0.00	-	-	6.620913
-	0.05	-	-	6.671877
-	0.10	-	-	6.68163
-	0.10	0.0	-	5.81848
-	-	0.5	-	6.383257
-	-	1.0	-	6.681631
-	-	1.0	0.00	6.928744
-	-	-	0.05	6.681631
-	-	-	0.10	6.4515373

Table 3. Impacts of different parameters on stresses at the surface of the disk.

α	ϕ	λ	$A_1F'(0)$	$-A_1G'(0)$
0.00	0.1	1.0	0.30917	1.35526
0.05	-	-	0.25372	1.273895
0.10	-	-	0.21088	1.199551
0.05	0.00	-	0.25847	1.02623
-	0.05	-	0.25349	1.14358
-	0.10	-	0.24705	1.284292
-	0.10	0.0	0.44130	0.70957
-	-	0.5	0.31896	1.019131
-	-	1.0	0.247055	1.284292

The coefficients A_i (i = 1, 2, 3, 4) are given by

$$A_1 = \frac{1}{(1-\phi)^{2.5}},\ A_2 = 1-(\phi)+\frac{\rho_p}{\rho_f}(\phi),$$

$$A_3 = \left(\frac{K_p + 2\phi\left(K_p - K_f\right) + 2K_f}{K_p - \phi\left(K_p - K_f\right) + 2K_f}\right),\ A_4 = \frac{(\rho C)_p}{\left(\rho C\right)_f}\ \phi - (\phi - 1)\left(\rho C\right)_f.$$

2.3. Solution Methodology

The system of (13)–(17) is difficult to solve exactly; hence, numerical simulations were applied. Computationally, for the considered boundary value problem, we implemented a combination of the shooting method with the fourth-order Runge–Kutta algorithm to solve the ODEs at each step. Technically, we implemented Mathematica's NDsolve function. We should stress that the considered pairing of the shooting method with fourth-order Runge–Kutta integration is frequently chosen since it provides both speed and precision in several fluid flow problems; see, for instance, [32,33]. Additionally, NDsolve already has built-in support for this approach, making it straightforward to use. When used in conjunction with Mathematica's NDsolve function, the shooting method and fourth-order Runge–Kutta integration have several benefits, including high precision and stability in solving fluid flow equations, adaptability for handling a wide range of problems, speed, and efficiency in computation. The step size was taken to be 0.01 for all computations.

The results of the simulations were compiled in the form of graphs and tabular data. The values of the following model parameters were fixed as $\phi = 0.1$, $\lambda = 1.0$, $\epsilon = 1.0$, $Pr = 6.2, \alpha = 0.05$, and $\beta = 0.05$, unless stated otherwise. For the sake of the validity of the adopted numerical procedure, a brief comparison of a reduced case of the present study is provided with the results reported by Wahed and Emam [34]; see Table 4. This comparison was carried out using the thermophysical properties of CuO (copper oxide) instead of Cu, and both slip parameters were set equal to zero. This approach was adopted due to the unavailability of a study specifically related to copper, so we made use of the material properties of CuO for comparison purposes. It is important to note that we only utilized the values of material parameters corresponding to CuO, while the underlying mathematical expressions remained consistent for both copper and CuO. This approach allows us to draw meaningful comparisons even in the absence of direct data for copper nanofluids.

Also, it is noteworthy that the effective viscosity contribution in the porous medium term was neglected for the sake of comparison (i.e., assuming $A_1 \to 1$). Ignoring this term does not give rise to the correct impacts of the porosity parameter on the velocity or, hence, the temperature. For nanofluids, where the viscosity is altered by the nanoparticles' volume fraction, this volume fraction also appears as a factor within the porous medium's

dimensionless equations. These factors were accounted for in the present study to give rise to more accurate results and provide a reference for future research in this direction.

Table 4. Comparison of a reduced case of the present study using CuO nanoparticles with the study by Wahed and Emam [34] for $\lambda = 0.5$.

Studies	$F'(0)$
$M = m = 0$ from Wahed and Emam [34] for CuO nanoparticles.	0.29667
$\alpha = 0$ and $\beta = 0$ for the present study, considering CuO nanoparticles and neglecting effective viscosity effects on the porous medium	0.296266

3. Results

This section presents the results of our numerical simulation, which are shown as graphs (Figures 2–15) and tables (Tables 2–4). The figures show the temperature and velocity components as functions of coordinates for the variations in the key parameters. The tables present an analysis of the heat transfer rate and stresses at the surface of the disk. A short summary of the obtained results, the considered ranges of the parameters, and a list of the corresponding figures are present in Table 5.

Table 5. Summary of the theoretical investigation of the dependence of the temperature and velocity components on key model parameters (for details related to each figure, see the text).

Parameter	Range	Its Effect is Examined on:	Illustrations
Velocity slip parameter, α	$0 \leq \alpha \leq 0.15$	Temperature $\theta(\zeta)$ and velocities $F(\zeta)$, $G(\zeta)$, $H(\zeta)$	Figures 2 and 7–9
Temperature slip parameter, β	$0 \leq \beta \leq 0.15$	Temperature $\theta(\zeta)$	Figure 3
Porosity parameter, λ	$0 \leq \lambda \leq 0.06$	Temperature $\theta(\zeta)$ and velocities $F(\zeta)$, $G(\zeta)$, $H(\zeta)$	Figures 4 and 13–15
Heat generation parameter, ϵ	$0 \leq \epsilon \leq 2$	Temperature $\theta(\zeta)$	Figure 5
Nanoparticle volume fraction, ϕ	$0 \leq \phi \leq 0.09$	Temperature $\theta(\zeta)$ and velocities $F(\zeta)$, $G(\zeta)$, $H(\zeta)$	Figures 6 and 10–12

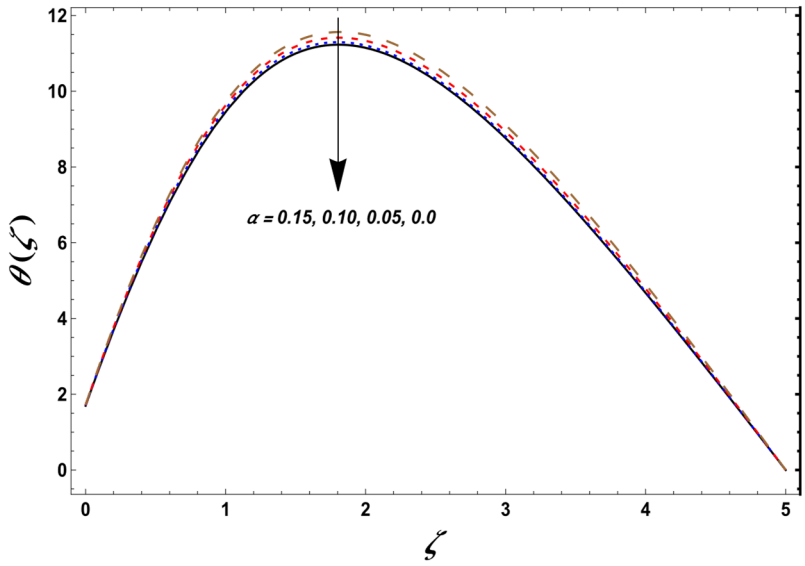

Figure 2. Impact of the velocity slip parameter (α) on the dimensionless temperature. The other parameters are $\phi = 0.1$, $\lambda = 1.0$, $\epsilon = 1.0$, $Pr = 6.2$, and $\beta = 0.05$.

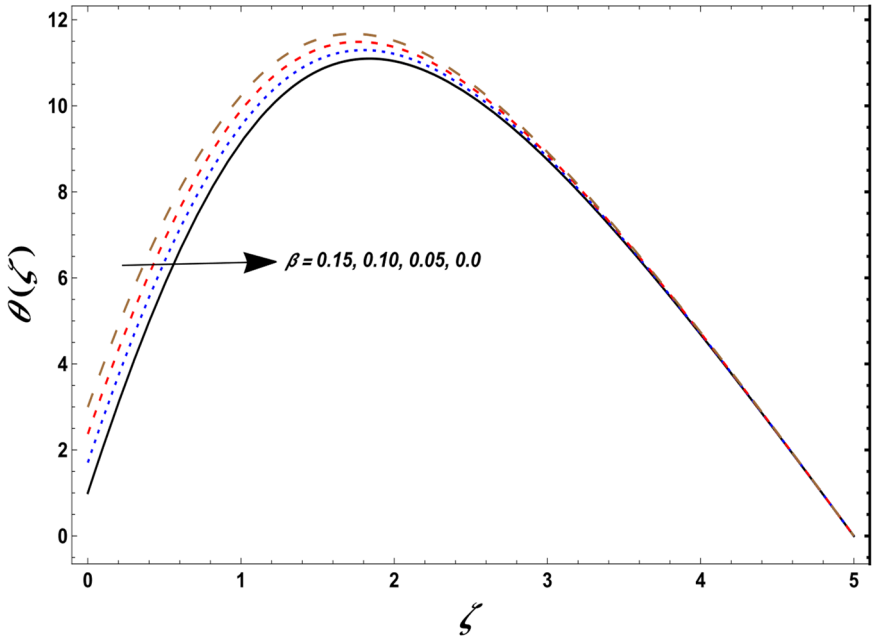

Figure 3. Impact of the temperature slip parameter (β) on the dimensionless temperature. The other parameters are $\phi = 0.1$, $\lambda = 1.0$, $\epsilon = 1.0$, $Pr = 6.2$, and $\alpha = 0.05$.

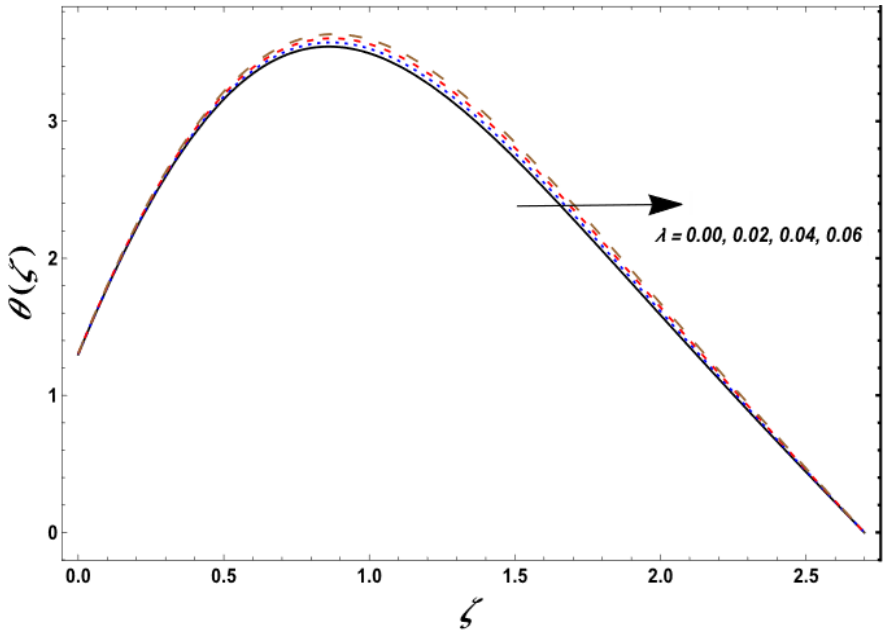

Figure 4. Impact of the porosity parameter (λ) on the dimensionless temperature. The other parameters are $\phi = 0.1$, $\epsilon = 1.0$, $Pr = 6.2$, $\alpha = 0.05$, and $\beta = 0.05$.

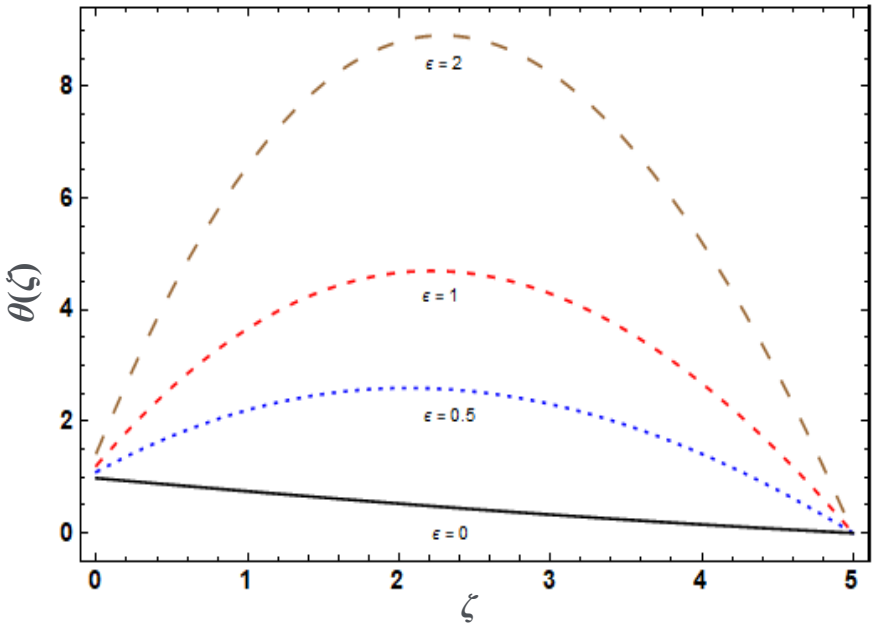

Figure 5. Impact of the heat generation parameter (ϵ) on the dimensionless temperature. The other parameters are $\phi = 0.1,\ \lambda = 1.0,\ Pr = 6.2,\ \alpha = 0.05,$ and $\beta = 0.05$.

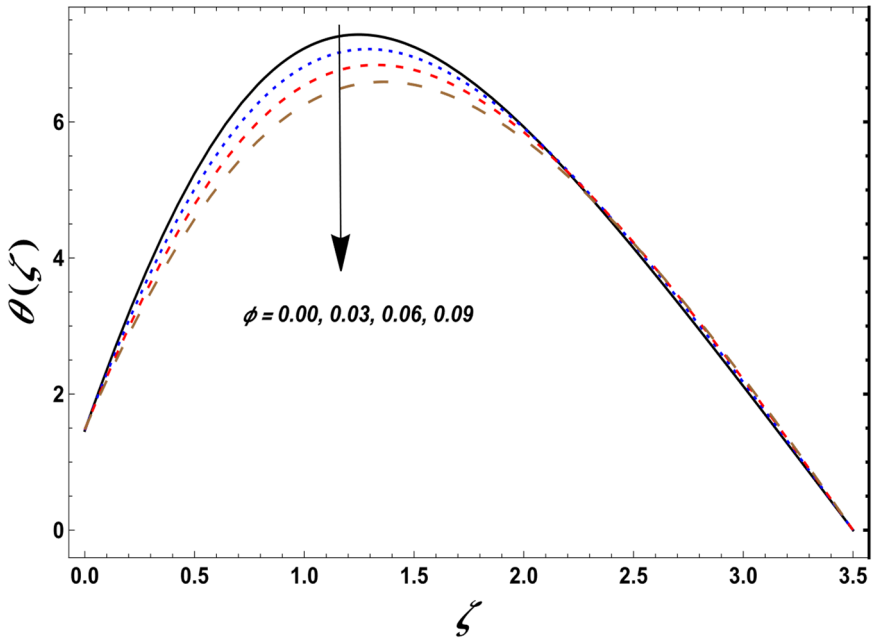

Figure 6. Impact of the nanoparticle volume fraction (ϕ) on the dimensionless temperature in the case of heat generation $(\varepsilon > 0)$. The other parameters are $\lambda = 1.0,\ \epsilon = 1.0,\ Pr = 6.2,\ \alpha = 0.05,$ and $\beta = 0.05$.

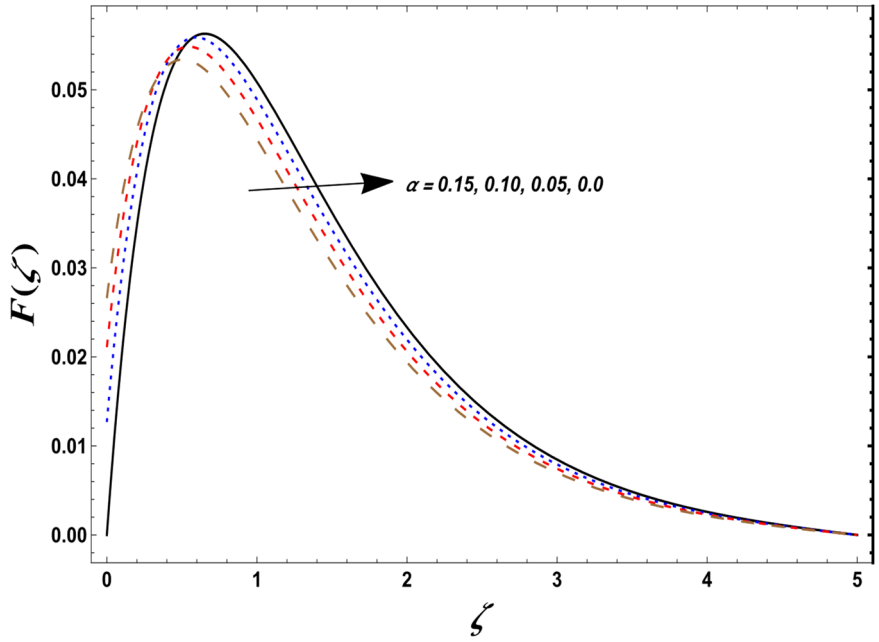

Figure 7. Impact of the velocity slip parameter (α) on the radial velocity component. The other parameters are $\phi = 0.1$, $\lambda = 1.0$, $\epsilon = 1.0$, $Pr = 6.2$, and $\beta = 0.05$.

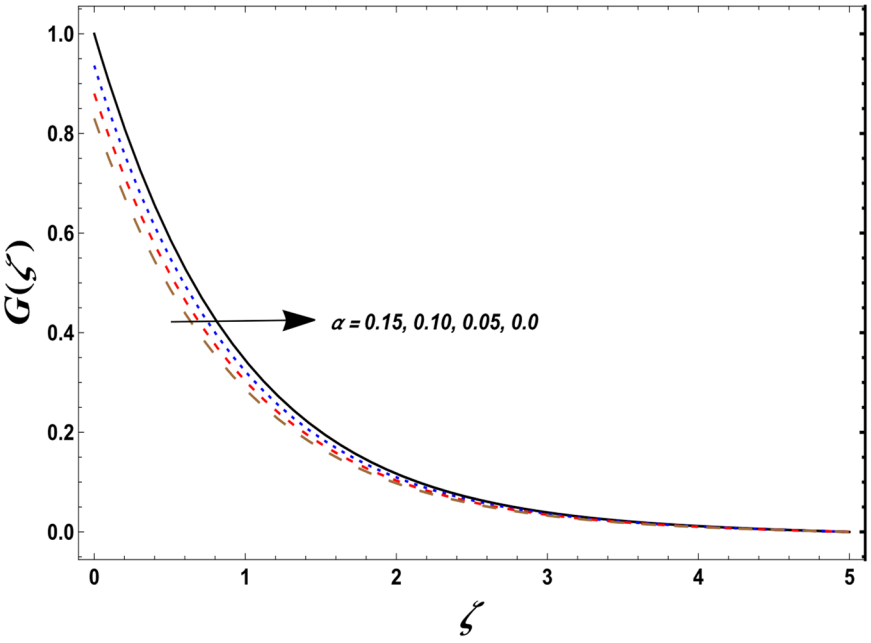

Figure 8. Impact of the velocity slip parameter (α) on the azimuthal velocity component. The other parameters are $\phi = 0.1$, $\lambda = 1.0$, $\epsilon = 1.0$, $Pr = 6.2$, and $\beta = 0.05$.

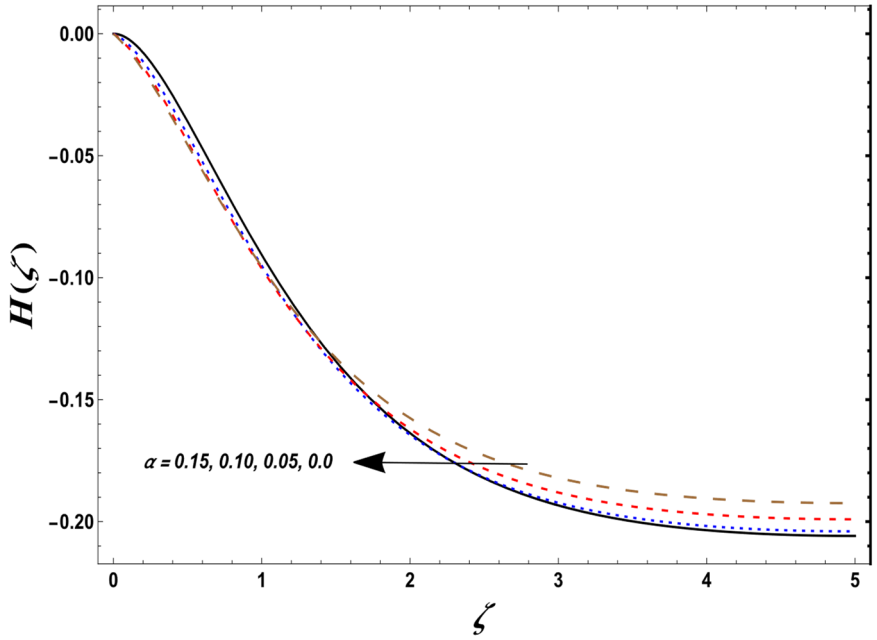

Figure 9. Impact of the velocity slip parameter (α) on the axial velocity component. The other parameters are $\phi = 0.1$, $\lambda = 1.0$, $\epsilon = 1.0$, $Pr = 6.2$, and $\beta = 0.05$.

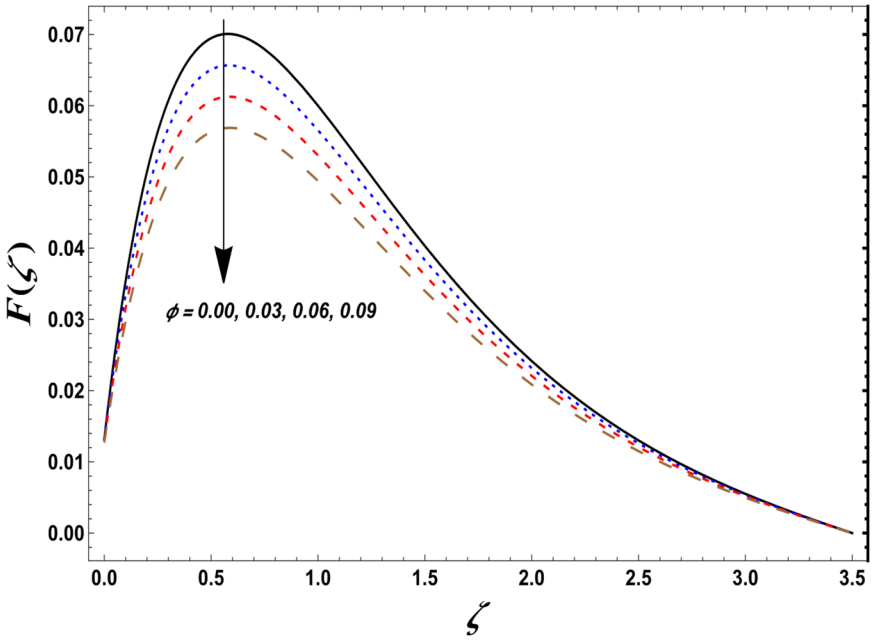

Figure 10. Impact of the nanoparticle volume fraction (ϕ) on the radial velocity component. The other parameters are $\lambda = 1.0$, $\epsilon = 1.0$, $Pr = 6.2$, $\alpha = 0.05$, and $\beta = 0.05$.

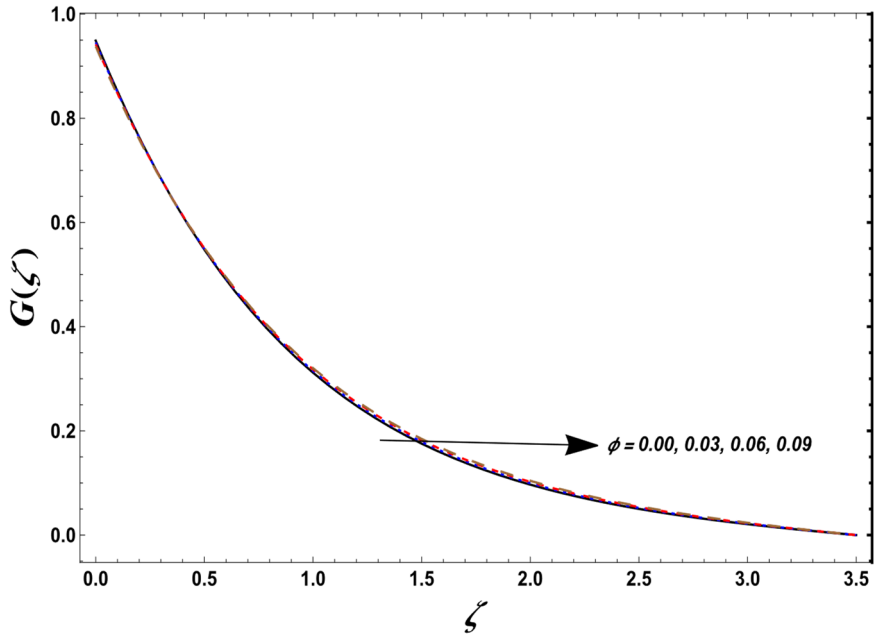

Figure 11. Impact of the nanoparticle volume fraction (ϕ) on the azimuthal velocity component. The other parameters are $\lambda = 1.0$, $\epsilon = 1.0$, $Pr = 6.2$, $\alpha = 0.05$, and $\beta = 0.05$.

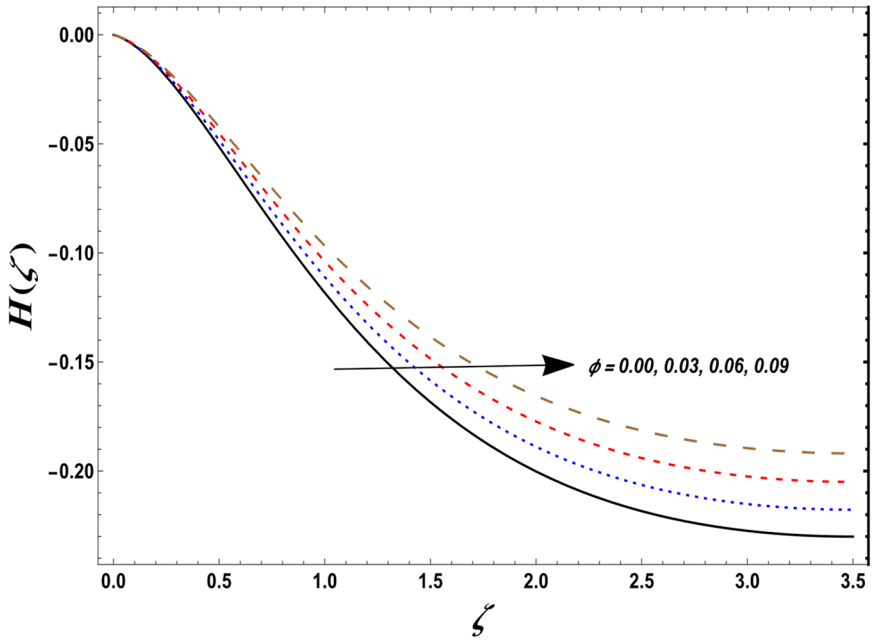

Figure 12. Impact of the nanoparticle volume fraction (ϕ) on the axial velocity component. The other parameters are $\lambda = 1.0$, $\epsilon = 1.0$, $Pr = 6.2$, $\alpha = 0.05$, and $\beta = 0.05$.

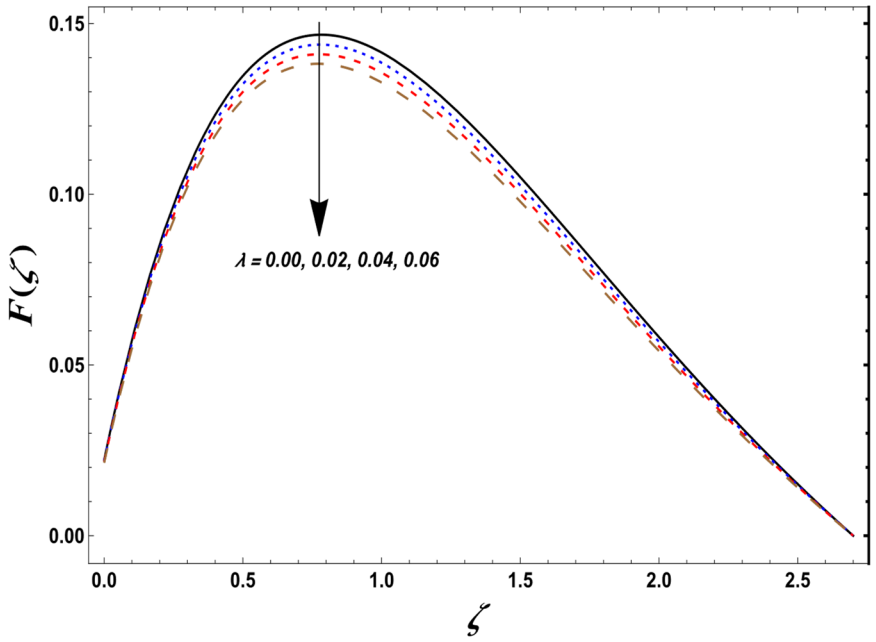

Figure 13. Impact of the porosity parameter (λ) on the radial velocity component. The other parameters are $\phi = 0.1$, $\epsilon = 1.0$, $Pr = 6.2$, $\alpha = 0.05$, and $\beta = 0.05$.

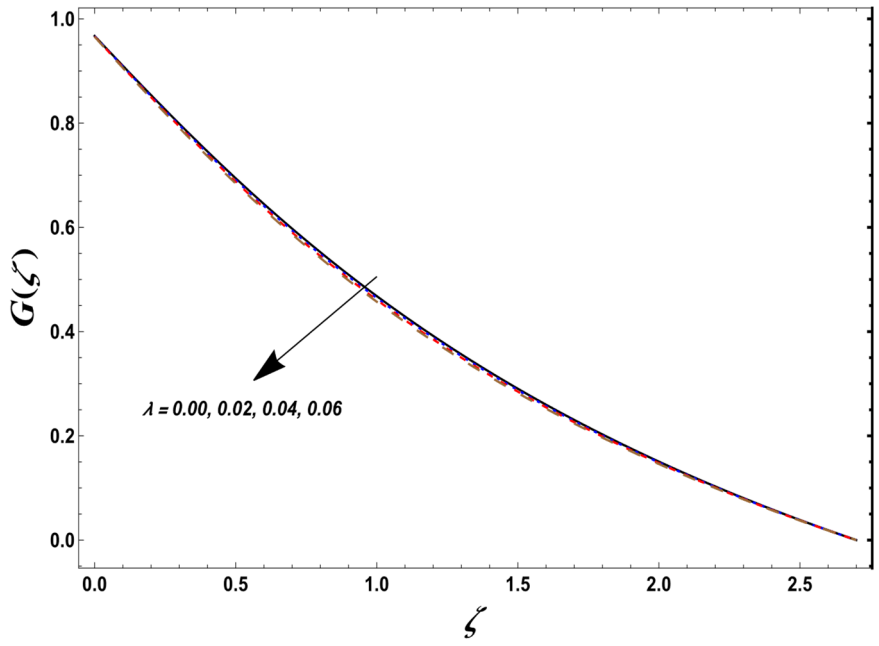

Figure 14. Impact of the porosity parameter (λ) on the azimuthal velocity component. The other parameters are $\phi = 0.1$, $\epsilon = 1.0$, $Pr = 6.2$, $\alpha = 0.05$, and $\beta = 0.05$.

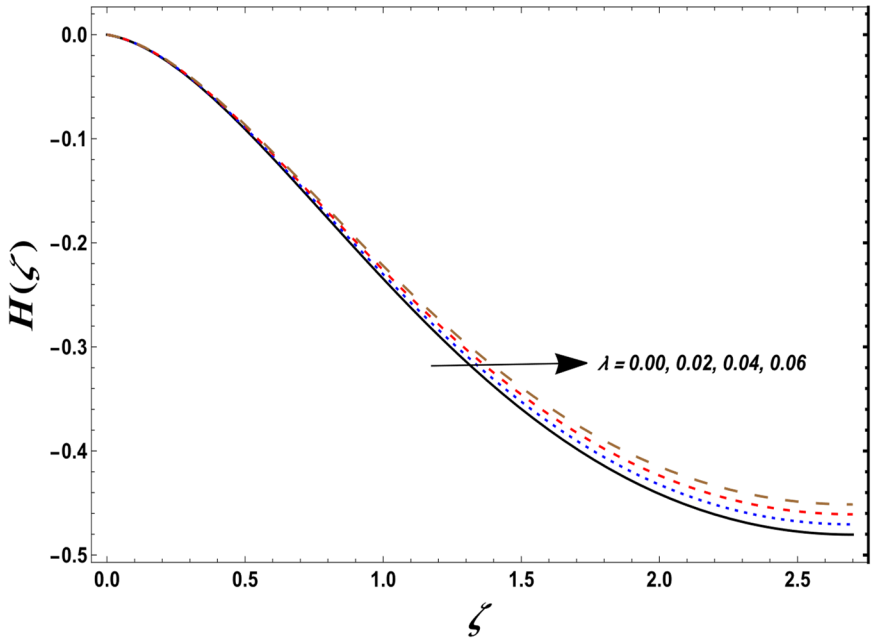

Figure 15. Impact of the porosity parameter (λ) on the axial velocity component. The other parameters are $\phi = 0.1$, $\epsilon = 1.0$, $Pr = 6.2$, $\alpha = 0.05$, and $\beta = 0.05$.

The Results section is divided into two subsections demonstrating the heat transfer analysis, which shows the temperature and heat transfer rate (Section 3.1), and the flow behavior analysis for the determination of the velocity components and stresses at the surface (Section 3.2).

3.1. Heat Transfer Analysis

We found that the slip boundary condition is pivotal in shaping velocity and temperature distributions in the nanofluid flow problem, particularly near the interface between the fluid and the disk surface. Grasping these effects is imperative for precise predictions of fluid behavior and heat transfer characteristics. Figures 2 and 3 illustrate the spatial distribution of temperature and demonstrate the impact of the slip parameter. In relation to temperature distributions, slip boundary conditions significantly influence heat transfer rates between the nanofluid and the disk surface. The temperature profiles near the surface depend on the slip parameters. As illustrated in Figure 2, temperatures are lower in the absence of a velocity slip, but they increase with a higher velocity slip. While this increase may seem relatively minor, it could be of concern in scenarios demanding precise simulations and practical applications. Enhanced convective heat transfer, resulting from an increased velocity slip parameter, contributes to this rise in temperature. The temperature of the nanofluid increases with a rise in the temperature slip parameter (see Figure 3). This increase is more pronounced compared to the effect observed with the velocity slip parameter and is particularly influential near the surface of the disk. Variations in the temperature slip parameter have an impact on temperature distributions, potentially altering thermal boundary layer thicknesses and heat transfer rates.

Figure 4 depicts that a nanofluid flowing through a uniform porous medium possesses a higher temperature than that in the absence of such a medium. Moreover, the temperature rises as the porosity of the medium increases. From a physical point of view, the increase in the porosity parameter causes an increase in viscous dissipation, which leads to heating of the fluid and an increase in the temperature. Figure 5 highlights the influence of the heat generation parameter on the temperature. One can see from this figure that the temperature of the nanofluid is largely influenced by heating. We also theoretically explored the influence of the nanoparticle volume fraction on the temperature of the nanofluid. The results of the simulations are shown in Figure 6. One can see that the temperature of the

nanofluid decreases for a higher volume fraction of nanoparticles in the presence of a heat source.

Table 2 presents numerical values for the heat transfer rate between the surface and the fluid adjacent to it. The results depict that the heat transfer rate at the surface increases with a rise in the velocity slip parameter, the nanoparticle volume fraction, and the porosity of the medium. Such an increase is more dominant in the case of the porosity parameter. The heat transfer rate is seen to decrease considerably for higher values of the temperature slip parameter.

3.2. Analysis of the Velocity and Stresses

Figures 7–15 illustrate the behavior of the fluid velocity components as key system parameters are varied. Particularly, Figures 7–9 depict the variations in the radial, azimuthal, and axial velocities with changes in the velocity slip parameter. The slip boundary conditions at the nanofluid–disk interface significantly influence the velocity profiles near the disk's surface. Typically, the presence of slip conditions results in an increase in the radial velocity, while the azimuthal and axial velocity components decrease. This effect is most pronounced near the disk's surface, where the slip effects are most influential. Away from the disk, the impact of the slip conditions on the velocity distributions diminishes. This can be attributed to the decreasing influence of slip effects as the distance from the disk increases.

The nanoparticle volume fraction has a considerable impact on the radial and axial components of the velocity, while it has only a minor influence on the azimuthal component (see Figures 10–12 for detail). The radial component of the velocity exhibits a considerable decrease for higher volume fractions of copper nanoparticles. From a physical point of view, an increase in the nanoparticle volume fraction signifies that the mixture becomes more viscous, and hence the velocity of the flow diminishes. On the other hand, the axial component shows an increase for larger values of ϕ. Such an increase becomes more pronounced at large distances from the disk.

We find that a nanofluid flowing through a porous medium possesses a lower radial velocity (see Figure 13) due to the increase in the resistance of the flow due to elements of the porous medium, but it has a slightly higher axial velocity (see Figure 15). Thus, it is important to note that with an increase in the nanoparticle fraction, the magnitude of the radial component of the velocity decreases, reaching its highest value near the disk at the same axial distance but remaining lower than the non-slip case reported in previous studies [23]. Additionally, the velocity tends to decrease as the distance from the disk increases, achieving zero magnitude earlier compared to the non-slip conditions [23]. This behavior is mainly attributed to the increased viscosity due to the higher nanoparticle volume fraction, resulting in centrifugal effects near the disk, propelling the fluid outward in the radial direction with higher velocities near the disk compared to farther locations.

On the other hand, the decrease in the azimuthal velocity is less prominent (see Figure 14) for higher values of the porosity parameter, suggesting very little impact on the velocity in the azimuthal direction. Importantly, the impact of the porosity parameter on all the velocity components is also perturbed by the nanoparticle volume fraction. We conclude that ignoring the impact of the effective viscosity along with the porosity parameter in mathematical models of nanofluids would give rise to less accurate results, as in this case, where the impact of the porous medium on the fluid's velocity is not perturbed by the nanoparticles. The magnitude of the axial velocity becomes higher with an increase in the nanoparticle fraction, and it significantly decreases as the distance from the disk increases, following a similar trend as in the non-slip case [23]. However, the axial velocity reaches a uniform pattern earlier than in the case of non-slip conditions [23], after a considerable reduction.

Finally, Table 3 specifies our simulation results on how the stresses at the surface are influenced by the velocity slip parameter, the porosity parameter, and the volume fraction of nanoparticles. The outcome of the simulation reveals that an increase in the

velocity slip parameter leads to a reduction in both radial and azimuthal stresses. From the physical point of view, the slip at the surface occurring due to the polished disk surface reduces the stresses and hence can aid in reducing wear at the surface of the disk. Moreover, such stresses behave oppositely when the nanoparticle volume fraction and the porosity parameter are assigned higher values.

4. Discussion

Here, we theoretically explore heat transfer in the flow of a nanofluid generated by a rigid rotating disk through a uniform porous medium in the presence of a heat source. The novelty of this study is the assumption that the disk surface is well polished. Polishing the surface of the disk facilitates the slip, and hence it reduces the stresses at the surface of the disk, which was missed in some previous studies of nanofluid modeling. Mathematically, the above-mentioned assumption signifies that we need to implement the velocity and temperature slip boundary conditions using the effective viscosity and the thermal conductivity. In our computer simulations, we used the physical parameters of the copper–water nanofluid system, which has important practical applications in physics and engineering [23–26]. We should stress that despite a few existing studies including slip effects for the flow of a nanofluid over a rotating rigid disk (e.g., [27–30]), the effects of viscosity and thermal conductivity of nanofluids have not been well addressed. Therefore, this study was supposed to partly fill the existing gap in knowledge and provide a reference point for future investigations of similar flow configurations of nanofluids. The modeling results could potentially help in optimizing heat transfer processes in diverse engineering systems, particularly in thermal engineering, to create more accurate and efficient heat transfer systems. The major outcomes of this study are the following.

For the slip boundary conditions considered, the axial velocity increases with a larger value of the nanoparticle fraction. However, it decreases significantly with the distance from the disk, similar to the trend observed in the non-slip case studied in [23]. Moreover, the axial velocity reaches a uniform pattern earlier than in the non-slip conditions after a considerable reduction. Increasing the nanoparticle fraction leads to a decrease in the radial component of velocity, with its highest value observed near the disk at the same axial distance, yet it remains lower than in the non-slip case [23]. The axial velocity diminishes as the distance from the disk increases, approaching zero magnitude earlier than in the non-slip conditions. This is primarily due to an increased viscosity resulting from the higher nanoparticle volume fraction, which induces centrifugal effects near the disk, causing the fluid to move outward, with higher velocities near the disk compared to distant regions. The simulation shows that the radial velocity component shows an increase, whereas the azimuthal and axial velocity components depict a decrease as the velocity slip parameter is assigned higher values, for example, due to an increase in the nanoparticle fraction in the porous medium.

Our model-based observation is that the temperature of the nanofluid increases with a corresponding increase in the velocity and temperature slip parameters, as well as the porosity of the environment, although the observed increase is somewhat minor. Importantly, adding nanoparticles to the system results in a decrease in the temperature, especially in the presence of a heat source. The physical explanation for this effect is an increase in heat transfer across the system due to the higher conductivity of the fluid. In this case, the outflow of energy from the location with the maximum temperature becomes faster. This finding, however, differs from the one reported in a previous study of a similar system of copper–water nanofluids, where increasing the number of nanoparticles generally caused a temperature increase [23].

The above-mentioned discrepancy between the results indicates that adding nanoparticles to a fluid may produce various outcomes in terms of alterations in the spatial temperature distribution. This, unfortunately, does not provide us with some simple and unambiguous conclusion regarding what exactly one should expect after adding nanoparticles: whether it has a positive or a negative impact on the temperature distribution. This is

quite contrary to previous studies, which have suggested the temperature effects of nanofluids to be fairly straightforward [8,13,34]. Therefore, although the addition of nanoparticles technically enhances the heat transfer rate, whether there is an increase or a decrease in the temperature would depend on a particular scenario (slip/non-slip conditions), the presence of heating sources, as well as the temperature of the external environment. More studies would be needed to elucidate this problem.

We also found that the impact of the nanoparticle volume fraction on the temperature largely depends on the intensity of the heat source. In particular, an increase in heating results in the occurrence of a pronounced maximum temperature at an intermediate distance. We revealed a combined effect, where the impact of the variation in the nanoparticle volume fraction on the temperature's spatial distribution was strongly influenced by the presence of a heat source and the strength of heating.

As a possible limitation of this study, we should mention the following. The modeling results obtained for copper–water nanofluids might not be directly applicable to systems of other nanofluids possessing distinctly different thermal and fluid dynamic behaviors. For example, well-known carbon nanotube (CNT)–water nanofluids exhibit distinct characteristics due to the unique properties of carbon nanotubes. It is known that CNTs can form networks or agglomerates within a fluid, affecting its rheological properties and thermal conductivity [35]. Additionally, the aspect ratio and surface chemistry of carbon nanotubes can influence their dispersion and interaction with a fluid, leading to different flow and heat transfer behaviors compared to copper–water nanofluids. Therefore, a separate investigation of heat transfer is required for network-forming nanofluids.

5. Conclusions

In our study, numerical simulations were conducted to analyze heat transfer in the flow of a copper–water nanofluid induced by a rigid rotating disk through a uniform porous medium in the presence of a heat source/sink and velocity and temperature slip conditions. The key findings of the study are summarized as follows:

- The temperature of the nanofluid exhibits an increase with higher values of velocity and temperature slip parameters.
- The effective viscosity and thermal conductivity of the nanofluid play a role in accounting for the slip effects within the system.
- The influence of the nanoparticle volume fraction on the nanofluid's temperature is expected to be particularly notable in the presence of a heat source.
- Higher values of the velocity slip parameter lead to an increase in the radial velocity component, accompanied by a decrease in the azimuthal and axial velocity components.
- Increasing the nanoparticle fraction results in a decrease in the radial velocity component, with peak values observed near the disk at the same axial distance, which are lower than those under non-slip conditions. Additionally, the velocity decreases as the distance from the disk increases, reaching zero magnitude sooner than under non-slip conditions due to heightened viscosity resulting from an increased nanoparticle volume fraction. This induces centrifugal effects near the disk and results in higher fluid velocities near the disk compared to distant regions.
- The axial velocity reaches a uniform pattern earlier than under non-slip conditions, following a considerable reduction.

Overall, we conclude that explicitly taking into account the slip boundary conditions for a well-polished rotating disk should provide more accurate results in predicting velocity and temperature fields, as they have previously been obtained while assuming a simplified non-slip boundary condition for most nanofluids. This concerns both the quantitative accuracy of predictions and the understanding of the dependence of the temperature and velocity fields on key parameters (e.g., the volume fraction of the nanofluid, the porosity of the medium, the heat generation rate).

Possible important extensions of this study might include considering other types of base fluids with thermal properties that vary with temperature. Moreover, one can also

consider unsteady, non-symmetric flows of nanofluids to include possible critical effects which might be missed in this study when considering a simple steady flow with radial symmetry. Finally, it was reported earlier that the thermal conductivity of nanofluids is generally affected by the shape of nanoparticles [36]. Also, in the case where particles form irregular nanoclusters, cluster size and morphology may have strong effects on the temperature of the boundary layer and heat transfer in nanofluids. For example, smaller clusters usually have higher surface-to-volume ratios, which can potentially lead to enhanced interactions with the surrounding fluid and potentially increase heat transfer rates. Therefore, it would be important to explore other shapes of nanoparticles (here, we considered particles of a spherical shape) and the effect of the presence of nanoclusters on the heat transfer characteristics of copper–water nanofluids.

Author Contributions: Conceptualization, N.A.M.A. and A.M.; methodology, A.M.; software, N.A.M.A.; validation, N.A.M.A.; formal analysis, N.A.M.A.; investigation, N.A.M.A.; writing—original draft preparation, N.A.M.A. and A.M.; supervision, A.M.; project administration, A.M. All authors have read and agreed to the published version of the manuscript.

Funding: This research received no external funding.

Data Availability Statement: The original contributions presented in the study are included in the article, and further inquiries can be directed to the corresponding author.

Acknowledgments: We authors would like to thank Aldo Rona from the University of Leicester, UK, for his very insightful comments. The authors highly appreciate the instructive comments of four anonymous reviewers.

Conflicts of Interest: The authors declare no conflicts of interest.

References

1. Wong, K.V.; De Leon, O. Applications of nanofluids: Current and future. *Adv. Mech. Eng.* **2010**, *2*, 519659. [CrossRef]
2. Choi, S.U.S.; Eastman, J.A. Enhancing thermal conductivity of fluids with nanoparticles. *ASME Int. Mech. Eng. Conger. Exposition* **1995**.
3. Buongiorno, J. Convective transport in nanofluids. *ASME J. Heat Transf.* **2006**, *128*, 240–250. [CrossRef]
4. Tiwari, R.K.; Das, M.K. Heat transfer augmentation in a two-sided lid-driven differentially heated square cavity utilizing nanofluids. *Int. J. Heat Mass Transf.* **2007**, *50*, 2002–2018. [CrossRef]
5. Nield, D.A.; Kuznetsov, A.V. Thermal instability in a porous medium layer saturated by a nanofluid: A revised model. *Int. J. Heat Mass Transf.* **2014**, *68*, 211–214. [CrossRef]
6. Abbasi, F.M.; Hayat, T.; Alsaedi, A. Peristaltic transport of magneto-nanoparticles submerged in water: Model for drug delivery system. *Phys. E Low-Dimens. Syst. Nanostructures* **2015**, *68*, 123–132. [CrossRef]
7. Abbasi, F.M.; Hayat, T.; Ahmad, B. Peristalsis of silver-water nanofluid in the presence of Hall and Ohmic heating effects: Applications in drug delivery. *J. Mol. Liq.* **2015**, *207*, 248–255. [CrossRef]
8. Cai, C.-J.; Shen, Z.-G.; Zheng, Y.-H.; Xing, Y.-S.; Ma, S.-L. A novel technology for powder dispersion and surface modification. *J. Mater. Sci.* **2007**, *42*, 3745–3753. [CrossRef]
9. Zou, H.; Chen, C.; Zha, M.; Zhou, K.; Xiao, R.; Feng, Y.; Qiu, L.; Zhang, X.; Wang, Z. A Neural Regression Model for Predicting Thermal Conductivity of CNT Nanofluids with Multiple Base Fluids. *J. Therm. Sci.* **2021**, *30*, 1908–1916. [CrossRef]
10. Mishra, S.; Mondal, H.; Behl, R.; Salimi, M. The Impact of Thermal Radiation on Mixed Convective Unsteady Nanofluid Flow in a Revolving Vertical Cone. *Mathematics* **2024**, *12*, 349. [CrossRef]
11. Peter, F.; Sambath, P.; Dhanasekaran, S. Numerical Investigation of Radiative Hybrid Nanofluid Flows over a Plumb Cone/Plate. *Mathematics* **2023**, *11*, 4331. [CrossRef]
12. Izadi, M.; Sheremet, M.A.; Mehryan, S.A.M. Natural convection of a hybrid nanofluid affected by an inclined periodic magnetic field within a porous medium. *Chin. J. Phys.* **2020**, *65*, 447–458. [CrossRef]
13. Ramesh, G.K.; Aly, E.H.; Shehzad, S.A.; Abbasi, F.M. Magnetized peristaltic transportation of Boron-Nitride and Ethylene-Glycol nanofluid through a curved channel. *Int. J. Ambient. Energy* **2022**, *43*, 3228–3236. [CrossRef]
14. Abbasi, F.M.; Gul, M.; Shanakhat, I.; Anjum, H.J.; Shehzad, S.A. Entropy generation analysis for magnetized peristaltic movement of nanofluid through a non-uniform asymmetric channel with variable thermal conductivity. *Chin. J. Phys.* **2022**, *78*, 111–131. [CrossRef]
15. Rauf, A.; Mushtaq, T.; Javed, M.; Alahmadi, H.; Shehzad, S.A. Modeling and analysis of Bödewadt hybrid nanofluid flow triggered by a stretchable stationary disk under Hall current. *Case Stud. Therm. Eng.* **2023**, 103315. [CrossRef]
16. Datta, A.; Halder, P. Thermal efficiency and hydraulic performance evaluation on Ag-Al_2O_3 and SiC-Al_2O_3 hybrid nanofluid for circular jet impingement. *Arch. Thermodyn.* **2021**, *42*, 163–182.
17. Von Kármán, T. Uber laminare und turbulente reibung. *Z. Angew. Math Mech.* **1921**, *1*, 233–252. [CrossRef]

18. Cochran, W.G. The flow due to a rotating disk. *Proc. Camb. Philos. Soc.* **1934**, *30*, 365–375. [CrossRef]
19. Stuart, J.T. On the effects of uniform suction on the steady flow due to a rotating disk. *Q. J. Mech. Appl. Mech.* **1954**, *7*, 446–457. [CrossRef]
20. Turkyilmazoglu, M. Nanofluid flow and heat transfer due to a rotating disk. *Comput. Fluids* **2014**, *94*, 139–146. [CrossRef]
21. Turkyilmazoglua, M. Fluid flow and heat transfer over a rotating and vertically moving disk. *Phys. Fluids* **2018**, *30*, 063605. [CrossRef]
22. Mustafa, M. MHD nanofluid flow over a rotating disk with partial slip effects: Buongiorno model. *Int. J. Heat Mass Transf.* **2017**, *108*, 1910–1916. [CrossRef]
23. Alkuhayli, N.A.M. Enhancing the Heat Transfer Due to Hybrid Nanofluid Flow Induced by a Porous Rotary Disk with Hall and Heat Generation Effects. *Mathematics* **2023**, *11*, 909. [CrossRef]
24. Hussain, S.; Aziz, A.; Khalique, C.M.; Aziz, T. Numerical investigation of magnetohydrodynamic slip flow of power-law nanofluid with temperature dependent viscosity and thermal conductivity over a permeable surface. *Open Phys.* **2017**, *15*, 867–876. [CrossRef]
25. Ramzan, M.; Riasat, S.; Chung, J.D.; Chu, Y.-M.; Sheikholeslami, M.; Kadry, S.; Howari, F. Upshot of heterogeneous catalysis in a nanofluid flow over a rotating disk with slip effects and Entropy optimization analysis. *Sci. Rep.* **2021**, *11*, 120. [CrossRef] [PubMed]
26. Kumar, S.; Sharma, K. Entropy optimized radiative heat transfer of hybrid nanofluid over vertical moving rotating disk with partial slip. *Chin. J. Phys.* **2022**, *77*, 861–873. [CrossRef]
27. Khan, I. Transportation of hybrid nanoparticles in forced convective Darcy Forchheimer flow by a rotating disk. *Int. Commun. Heat Mass Transf.* **2021**, *122*, 105177. [CrossRef]
28. Abdulaziz, N.; Alkuhayli, M. Magnetohydrodynamic flow of copper-water nanofluid over a rotating rigid disk with Ohmic heating and Hall Effects. *J. Magn. Magn. Mater.* **2023**, *575*, 170709.
29. Karimipour, A.; Esfe, M.H.; Safaei, M.R.; Semiromi, D.T.; Jafari, S.; Kazi, S.N. Mixed convection of copper–water nanofluid in a shallow inclined lid driven cavity using the lattice Boltzmann method. *Phys. A Stat. Mech. Its Appl.* **2014**, *402*, 150–168. [CrossRef]
30. Santra, A.K.; Sen, S.; Chakraborty, N. Study of heat transfer due to laminar flow of copper–water nanofluid through two isothermally heated parallel plates. *Int. J. Therm. Sci.* **2009**, *48*, 391–400. [CrossRef]
31. Kargarsharifabad, H. Experimental and numerical study of natural convection of Cu-water nanofluid in a cubic enclosure under constant and alternating magnetic fields. *Int. Commun. Heat Mass Transf.* **2020**, *119*, 104957. [CrossRef]
32. Alahmadi, H.; Alkinidri, M.O. Exploring the Impact of Nanomaterials on Heat and Mass Transfer Properties of Carreau-Yasuda Fluid with Gyrotactic Bioconvection Peristaltic Phenomena. *Mathematics* **2023**, *11*, 1474. [CrossRef]
33. Iqbal, J.; Abbasi, F.M.; Alkinidri, M.; Alahmadi, H. Heat and mass transfer analysis for MHD bioconvection peristaltic motion of Powell-Eyring nanofluid with variable thermal characteristics. *Case Stud. Therm. Eng.* **2023**, *43*, 102692. [CrossRef]
34. Abdel-Wahed, M.S.; Emam, T.G. Effect of joule heating and hall current on MHD flow of a nanofluid due to a rotating disk with viscous dissipation. *Therm. Sci.* **2018**, *22*, 857–870. [CrossRef]
35. Wang, T.; Song, B.; Qiao, K.; Huang, Y.; Wang, L. Effect of dimensions and agglomerations of carbon nanotubes on synchronous enhancement of mechanical and damping properties of epoxy nanocomposites. *Nanomaterials* **2018**, *8*, 996. [CrossRef]
36. Zahmatkesh, I.; Sheremet, M.; Yang, L.; Heris, S.Z.; Sharifpur, M.; Meyer, J.P.; Ghalambaz, M.; Wongwises, S.; Jing, D.; Mahian, O. Effect of nanoparticle shape on the performance of thermal systems utilizing nanofluids: A critical review. *J. Mol. Liq.* **2021**, *321*, 114430. [CrossRef]